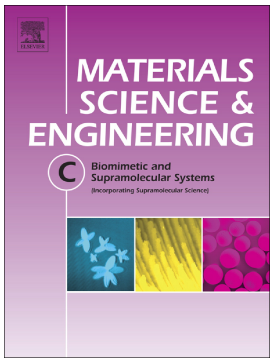

Synthesis and characterization of metals-substituted cobalt ferrite [Co(1−x)]MxFe2O4; (M=Zn, Cu, Mn; x=0,05)] nanoparticles as antimicrobial agents and sensors for Anagrelide determination in biological samples

M.I.A. Abdel Maksoud, Gharieb S. El-Sayyad, A.H. Ashour, Ahmed I. El-Batal, Mahmmoud S. Abd-Elmonem, Hassan A.M. Hendawy, E.K. Abdel-Khalek, Sh. Labib, E. Abdeltwab, M.M. El-Okr

PII:	S0928-4931(17)34472-7
DOI:	doi:10.1016/j.msec.2018.07.007
Reference:	MSC 8719
To appear in:	*Materials Science & Engineering C*
Received date:	14 November 2017
Revised date:	25 June 2018
Accepted date:	1 July 2018

Please cite this article as: M.I.A. Abdel Maksoud, Gharieb S. El-Sayyad, A.H. Ashour, Ahmed I. El-Batal, Mahmmoud S. Abd-Elmonem, Hassan A.M. Hendawy, E.K. Abdel-Khalek, Sh. Labib, E. Abdeltwab, M.M. El-Okr , Synthesis and characterization of metals-substituted cobalt ferrite [Co(1−x)]MxFe2O4; (M=Zn, Cu, Mn; x=0,05)] nanoparticles as antimicrobial agents and sensors for Anagrelide determination in biological samples. Msc (2018), doi:10.1016/j.msec.2018.07.007

Synthesis and characterization of metals-substituted cobalt ferrite $Co_{(1-x)}M_xFe_2O_4$; ($M = Zn, Cu, Mn$; $x = 0, 0.5$)] nanoparticles as antimicrobial agents and sensors for Anagrelide determination in biological samples

M.I.A. Abdel Maksoud[a], Gharieb S. El-Sayyad[b*],A. H. Ashour[a], Ahmed I. El-Batal[b],Mahmmoud S. Abd-Elmonem[c], Hassan A. M. Hendawy[c],E. K. Abdel-Khalek[d], , Sh. Labib[e], E. Abdeltwab[f], M.M. El-Okr[d].

[a]*Materials Science Lab., Radiation Physics Department, National Center for Radiation Research and Technology (NCRRT), Atomic Energy Authority, Cairo, Egypt.*

[b]*Drug Microbiology Lab., Drug Radiation Research Department, National Center for Radiation Research and Technology (NCRRT), Atomic Energy Authority, Cairo, Egypt.*

[c]*National Organization for Drug Control and Research (NODCAR), P.O. Box 29, Cairo, Egypt.*

[d]*Physics Department, Faculty of Science (Boys Branch), Al-Azhar University, Cairo, Egypt.*

[e]*Nuclear Chemistry Department, Hot Laboratories Center, Atomic Energy Authority, P.O. Box 13759, Cairo, Egypt.*

[f]*Physics Department, Faculty of Science (Girls Branch), Al-Azhar University, Cairo, Egypt.*

* Corresponding Author email address: Gharieb.Elsayyad@eaea.org.eg, adham_adham699@yahoo.com.

Abstract:

Nanocrystalline spinel ferrite nanoparticles $\left[M_xCo_{(1-x)}Fe_2O_4\ ;\ (\ M = Zn, Cu, Mn\ ;\ x =\ 0 \text{ and } 0.5\ )\right]$ like: Cobalt ferrite (CFO), Zinc Cobalt ferrite (ZCFO), Copper Cobalt ferrite (CCFO), and Manganese Cobalt ferrite (MCFO) modified carbon paste electrodes (CPE) were synthesized via sol–gel technique utilizing citric acid and ethylene glycol as a polymerization agent. The synthesized ferrite NPs were used as bi-functional smart biosensor, not only used to determination the drug Anagrelide-HCl (ANDH) in urine and serum samples, but also possesses antimicrobial potential against some pathogenic microbes, founded in the biological samples. The synthesized ferrite NPs were confirmed by XRD, FTIR spectroscopy, SEM, EDX, and elemental mapping images. Antimicrobial activities of ferrite NPs against selected urinary tract infected microbes were investigated. From XRD data and FTIR spectroscopy it is found that the average crystallite size is lies in the range 12.86 to 33.92 ± 1.5 nm, also the bond lengths R_A and R_B increase from 1.8986 to 1.9145 Å and from 2.0434 to 2.0606 Å respectively and Debye temperature θ_D lies in the range of 681.52–708.87 K. Our study describes the improvement of a screen-printed sensor, modified with ferrite NPs materials for rapid, sensitive and cost-effective quantification of ANDH present in the real samples such as blood serum samples, urine and in the pharmaceutical formulations. The results obtained postulate a linear regression between the ANDH charge density of peak current and its concentration in the range from (0.64 - 8.18 µg/ml) with DL 0.31 µg/ml and QL 0.94 µg/ml. Antimicrobial results indicated thatZCFO NPs were a novel antibacterial agent against *Klebsiella pneumoniae* (28.0 mm ZOI), and multidrug-resistant bacteria *Enterococcus faecalis* (27.0 mm ZOI). Additionally, ZCFO NPs were active against *Candida albicans* (18.0 mm ZOI) seems to be a smart antifungal agent. Therefore, ZCFO NPs can be used as applicant resources for industrial, medical, and biological applications.

Keywords:

Cobalt ferrite nanoparticles; XRD; Elemental Mapping Images; *Klebsiella pneumoniae;* Zone of Inhibition; Screen printed electrodes; Anagrelide-HCl.

Introduction

In current times, an accelerated advancement of nanotechnology becomes forced up an environment of distinct opportunities for manufacturing nano-materials of wanted shapes, particle size suitable for employment as antimicrobial biosensors for drugs determination and, drugs delivery, agriculture, and industrial fields [1].

Spinel ferrites, although more than half a century of knowledge and development of these materials have been passed, however, the materials of this group are still being studied extensively in nanostructures, where they have many interesting properties, with particular regard to their magnetic properties. Taking into consideration, the spinel ferrites are magnetic semiconductors, which used in widespread and diverse technological fields such as high density information storage materials, phase shifters, converters, inductors, low and high-frequency transformer cores, catalysts, electronic devices, ferrofluid, humidity sensors, magnetic resonance imaging, drug delivery, antenna materials and microwave absorption [2-14].

Among spinel ferrites, CFO is one of the best candidates compared to others spinel ferrites which has drawn considerable research attention in the last five decades due to its unique tunable physical properties such as comparatively large coercivity, high magneto crystalline anisotropy, and moderate saturation of magnetization. These unique properties have made CFO has enormous potential in many technologies, such as information storage system, microwave absorber, optoelectronics, magneto-electronics, catalyst studies, high sensitivity sensors and biotechnology [15-17]. Over and above, the spinel ferrites have been used to boost the sensitivity and the stability of biosensors for the detection of sundry analyses such as in clinical, food and environmental applications [18].

In recent years, research on sensing properties of ferrites has become very popular, Li S.*et al.*, [19] have successfully used ferrite NPs MFe_2O_4 (M=Mg, Ni, Cu; prepared using a hydro- thermal method), as senor to glucose detection in urine sample. Ferrite NPs used to catalyze H_2O_2 to produce hydroxyl radicals and also to catalyze the decomposition reaction of H_2O_2 into water and oxygen directly in the same condition.

Negahban S.*et al.*, [20] have reported the synthesis, characterization and dobutamine DB sensing characteristics using $MnZnFe_2O_4$ and ionic liquid as a modified carbon paste electrode. The sensor had two linear dynamic ranges in the range of 4.0–148.0 and 148.0–740.0 μmol/L DB with limit of detection 1.0 μmol/L DB. The proposed method was successfully applied to determine DB in urine and pharmaceutical samples.

Anagrelide hydrochloride (ANDH) 6, 7-dichloro-5, 10-dihydro-3H-imidazo [2, 1-b] quinazolin-2-one; hydrochloride) obtained the initial medicine approved by means of the FDA in 1997 for the thrombocytosis treatment (essential thrombocythemia), or excess creation of blood platelets[21]. Screen-printing electrode (SPE) is by all reports, a standout amongst the common supportive tactics allowing basic [22, 23] , swift and inexpensive sensors fabrication.

In the aspect of screen-printed terminals, biosensors have been generally used for discovery of important natural units, organic composites, pharmaceutical medications, and antigens. Electrochemical sensors in light of screen-printed are tuned into the needs of in situ screening devices, considering all the hardware needed for the electrochemical study is useful. They have all the important performance characteristics of sensors, between them the base sample form formation [23].

Microbial diseases remained one of the main reasons of mortality appears in the nineteenth century. Medicines especially antibiotics strongly decreased the death created by bacterial infections. Now, antimicrobial impacts are intensively considered due to an enormously growing bacterial defense toward extremely and regularly handled traditional medicines. It is quite complicated and the evolutionary methods ordinarily happen through antibiotic treatment, leading to the development of heritable immunity to antimicrobials [24].

In this regard, in our study we have confirmed the biological disposable sensor for ANDH as one of the application on novel unique multifunctional ferrite NPs with nominal composition[$M_xCo_{(1-x)}Fe_2O_4$; ($M = Zn, Cu, Mn$; $x = 0, 0.5$)] that, synthesized via sol–gel technology on the basis of ferrite electro sensitivity.

To our knowledge, this is the first report in the literature regarding the biological sensor using modified ferrite NPs for ANDH detection with the disposable sensor. On the other hand, the ferrite NPs owning encouraging excellent antimicrobial action upon chosen pathogenic microorganisms infected urinary tract and blood samples. By employing cyclic voltammetry (CV) and square wave (SV), in order to improve the analytical performance with more strong and facility of the aimed biological sensor, the exterior surface of the electrode consisted of a graphite and ZCFO NPs complex to advance the sensitivity and acceptance.

2. EXPERIMENTAL PROCEDURES

2.1. Materials

Media components are from (Oxoid) and (Difco). All chemicals and reagents used inthe following examinations received at the analytical type. Chemicals that used in ferrite NPs synthesis are ferric nitrate nonahydrate ($Fe(NO_3)_3 \cdot 9H_2O$; 98.0%), cobalt nitrate hexahydrate ($Co(NO_3)_2.6H_2O$;

99.5%), copper nitrate hexahydrate ($Cu(NO_3)_2.6H_2O$; 94.5%), manganese nitrate tetrahydrate ($Mn(NO_3)_2.4H_2O$; 98.0%) and zinc sulfate heptahydrate ($ZnSO_4.7H_2O$; 99%), citric acid (99.57%) and ethylene glycol ($C_2H_6O_2$; 99.8%).

2.2. Apparatus

A Metrohm pattern 797 VA Computrace electro analyzers were applied for voltammetric investigations. Three-electrode cell operations were employed to examine the cyclic and differential pulse voltammograms. An Ag/AgCl/KCl (3.0 mol L^{-1}) electrode, ferrite NPs printed and, a platinum wire were used as the reference, supporting and operating electrodes, respectively. A JENWAY 3510 pH-meter with a united glass electrode was appropriated for pH determinations.

2.3. Drug (Anagrelide-HCl) preparation

On the other hand, $1.0x10^{-3}$M ANDH solution, giving by the NODCAR of Egypt, was prepared daily by dissolving the adequate amount of ANDH in double distilled water (DDW) and diluted with the same solvent and was kept in a refrigerator at 4°C. More dilute solutions were prepared by serial dilution with water. Britton–Robinson (BR) buffer was used as electrolyte.

An adequate amount of 0.2 M NaOH was added to the BR buffer to obtain solutions of pH values varying from 2.0 to 10.0. Graphite powder (particle dimension20.0μm) was purchased from Sigma–Aldrich. A 0.04M BR buffer solution of pH 6.0 served as the supporting electrolyte solution.

Finally, the pharmaceutical sample, ANDH tablet (20.0 mg), was obtained from local drug stores. At all steps, Double distilled water (DDW) was used all the way through the experiment.

2.4. Synthesis of Ferrite NPs.

A sol-gel method has been used for the synthesis of spinel ferrite NPs with nominal composition[$M_xCo_{(1-x)}Fe_2O_4$; ($M = Zn, Cu, Mn$; $x = 0,0.5$)].

Stoichiometric amounts of the metal salts and citric acid (in the molar ratio 1:1 to precursor metal salts) were dissolved separately in minimum amount of distilled water (7.5 ml) for the hydrolysis reaction. The salt solutions were mixed and the resultant mixture was heated at 80°C under continuous stirring using a magnetic stirrer. After that, citric acid was added followed by the addition of ethylene glycol (10 ml) which was added as a polymerization agent and to initiate the gel formation. The resulting solution was continuously heated on the magnetic stirrer at 300°C in order to allow gel formation. Resulting gels were dried and crushed to obtain ferrite NPs powder [25].

2.5. Characterization of Ferrite NPs.

In this research, the complete structures of ferrite NPs have been identified by applying a completely computerized X-ray diffractometer, Shimadzu XRD- 6000, at NCRRT, Cairo, Egypt[26, 27]. The full validation of the received ferrite NPs has been produced by, determined the surface morphology of manufactured ferrites by using scanning electron microscopy (SEM) ZEISS, EVO-MA10 [28]. Besides, Energy-Dispersive X-ray spectra (EDX) BRUKER Nano GmbH D- 12489, 410-M (Berlin-Germany) was employed to investigate and determine the elemental form of the prepared ferrite NPs by used mapping method for supplying a full information about the purity of the synthesized ferrite NPs.

Eventually, FT-IR investigation was a significant plan that holds knowledge concerning chemical functional groups corresponding to the synthesized ferrite NPs [29]. The method was taken out

practicing a JASCO FT-IR 3600 Infra-Red spectrometer by used KBr technique .It was reported at a wave number spectrum of 400-4000cm^{-1}.

2.6. Preparation of the working electrodes

Polystyrene (which manufactured as follows 0.1gm cellulose acetate soluble in 10.0 ml of (1:1 acetone and cyclohexanone), 0.45 ng Graphite and 0.05gm of different ferrite NPs powders) over the PVC supports (each 5.0 × 10 mm) with diameter 1.0 mm. Thick films of the ferrite NPs revised ink were produced by grazing the ink over an etched stencil thickness 100.0 µm, electrode printing working area diameter 2.0 mm, with the support of the spatula presented with the screen-printing device. At last, an insulating layer (polystyrene) was reprinted across the SPE leaving the contact tip and molding range of 0.126 cm^2 as shown in figure (S1).

2.7. Electrochemical measurement

All operations were completed under ambient situations. Approximately, 5.0 mL quantity of 0.04 M BR buffer electrolyte having a satisfactory amount of ANDH was added to the voltammetric cell. The electrolyte suspension stayed degassed by pure nitrogen prior and throughout the electrochemical determinations. The work has been reported in the necessary growth potential for a particular limit of time, after that the suspension was mixed at about 2000 rpm during the particularized accumulation time.

On the other hand, stirring was arrested and was released to determine rest for 4.0 seconds, the scan was taken out towards positive potentials across the series 0.3 to 1.0V, and the signal voltammograms were reported. The test parameters were: voltage step, 6.5 mV; frequency, 50 Hz; amplitude 20 mV; and sweep rate 65 mV s-1 for stripping square wave voltammetry (AS-SWV).

The optimizations are given to the greatest amount of peak flow. Before each determination, a current of N_2 was prevented for the electrolyte in a voltammetric cell for 30 seconds to restore the electrode outside by the elimination of adsorbed particles; all the electrochemical investigations were performed at an ambient temperature.

2.8. Capsule Analysis

Five tablets of ANDH (20.0 mg) were ground fine in a glass mortar. An adequate quantity of the crushed particles compatible with a concentrated suspension of 1.0 mg mL^{-1} was carefully balanced and suspended in double distilled water. Additionally, the flask contents were sonicated for 40.0 minutes till full dissolved .The extract was isolated by filtration with a 0.45μm syringe filter and the filtrate was carried out to a 50.0 ml container and terminated to a volume with distilled water. The performing stock was developed by using suitable aliquots from the stock and diluted with distilled water for, support the standard interest design.

2.9. Spiked serum Analysis

Approximately, 0.3 mL $ZnSO_4$ (5.0%), and 0.5 ml ethanol were associated with 0.3 ml serum and, centrifuged for 5.0 min. at 4500 rpm. An aliquot (1.0 ml) of the clear superannuated was combined with 9.0 ml of the electrolyte suspension of BR buffer. The suspension was agitated for 3.0 min. and spiked with 50.0 ng/ml of ANDH. After that, follows the design demonstrated earlier.

2.10. Analysis in Spiked Urine

Samples of urine were collected from healthy volunteers without any processing; but, they are diluted by 50.0 times with 0.04 M BR buffer (pH 7.0). The dilution can reduce the medium

influence of original samples. Sufficient amount of ANDH was suspended in BR buffer (pH 7.4) to achieve the stock solution about 5µg/ml concentration. Additionally, ANDH were added to 5.0 ml diluted urine Therefore, the calibration carve were considered to plot at the popular peak against the drug concentration.

2.11. Antimicrobial potential of metals substituted CFO NPs

The preferred metal substituted cobalt ferrite NPs, synthesized by citric acid and ethylene glycol were dispersed in dimethyl sulfoxide (DMSO) to prepare a stock solution of final 1000 ppm concentration. They examined for the antimicrobial performance, using the agar disc diffusion method[30].

The bacterial inoculums were adjusted at 0.5 McFarland (1–2) $\times 10^8$ CFU/ml, using UV-Vis. spectrophotometer at 600 nm. On the other hand, the yeast inoculum was set at 0.5 McFarland (1–5) $\times 10^6$ CFU/ml.

All examined ferrite NPs and DMSO were tested upon different isolates of multidrug-resistant bacteria obtained kindly from Drug Microbiology laboratory, Drug Radiation Research department, NCRRT, Atomic Energy Authority. Tested pathogens include, Gram-positive bacteria (*Staphylococcus epidermidis*, *Staphylococcus aureus*; MRSA, and *Enterococcus faecalis*) and Gram-negative bacteria (*Acinetobacter baumannii*, *Enterobacter cloacae* and *Escherichia coli*).

The multidrug-resistant bacteria were investigated and, identified by Vitek® two systems (bioMarieux, Marcy-LEtoile, France)[31]. Moreover, all remained resistant to antibiotics particularly, Ampicillin, Colistin, Cephalexin, Piperacillin-Tazobactam, Ceftazidime, Gentamycin, Cefapirin, Cefotaxime, Cefoxitin, Meropenem, and Imipenem.

Additionally, ferrite NPsand DMSO were checked for the antibacterial potential toward standard strains of Gram-positive bacteria (*Bacillus subtilis* ATCC 6633), and Gram-negative bacteria (*Klebsiella pneumoniae* ATCC 4352 and *Pseudomonas aeruginosa* ATCC 27853).

Furthermore, an antifungal effect was investigated against unicellular fungi (*Candida albicans* ATCC 10231).The growth repression of all tested microbial strains, that some of them may infect the urinary tract of mammals was estimated by Zone of Inhibition (ZOI) after 24 hrs. plates incubation [29].

Conventional antibiotic discs (6.0 mm diameter) like Amoxicillin/Clavulanic Acid (AMC; 20/10 µg/ml), and Nystatin (NS 100; 100 µg/ml)[32],were chosen to evaluate the effect of the synthesized ferrite NPs.

3. Results and discussions:

3.1. Material characterization:

3.1.1. X- ray analysis

In this study the structure of CFO and metals substituted CFO ferrite NPs have been characterized by using X-ray diffractometer. The mean crystallite size D was calculated utilize Scherer's equation[33].

$$D = \frac{0.9\lambda}{\beta \cos\theta} \qquad (1)$$

Where β is the full width at half maximum (FWHM) of the most intense peak (311).

The experimental lattice constant for cubic system was determined from the inter-planar spacing (d) by using the formula:

$$a_{exp.} = d_{hkl}\sqrt{(h^2 + k^2 + l^2} \quad (2)$$

Where $h, k and l$ are the Miller indices of the diffraction peaks (hkl).

XRD patterns of CFO, ZCFO, CCFO, and MCFO NPs as-obtained are given in figure 1 ,the most intense peaks were observed at the 2θ values of 18.28^0, 30.12^0, 35.54^0, 37.12^0, 43.13^0, 53.41^0, 56.89^0 , 62.62^0 and 73.75^0 are indexed as the reflection planes of (111), (220), (311), (222), (400), (422), (511), (440), and (533), respectively, indicated the presence of cubic spinel phase[34, 35].

……**Figure 1**…….

Table1showed the average crystallite size, lattice parameters and inter-planar spacing of the unit cell calculated from XRD data of metals substituted nano-crystalline CFO NPs.

…… **Table (1)** …….

Figure (S2) illustrates the variations in the average crystallite size of metals substituted CFO nano-crystalline samples. It is noticed that the average crystallite size decrease with an increase on the full width at half maximum(β).

The bond lengths on A and B sites can also be calculated for the present ferrite samples by using the following equations[36].

$$R_A = a\sqrt{3}\left(\delta + \frac{1}{8}\right) \quad (3)$$

$$R_B = a\left(\frac{1}{16} - \frac{\delta}{2} + 3\delta^2\right)^{1/2} \quad (4)$$

Where, $\delta = U - U_{ideal}$, δ is the deviation of the oxygen parameter, U is the positional parameter for the spinel ferrite (0.381 Å) and the U_{ideal} is (0.375 Å).

So, as to elucidate the effect of metals substituted cobalt ferrite shared (d_{AE}, d_{BE}) and unshared edges (d_{BEU}) are also calculated from XRD data [37, 38].

Table (S1) summarizes the variation of bond length values ferrite NPs. It can be seen that the R_A and R_B increase from 1.8986 to 1.9145 and from 2.0434 to 2.0606 respectively with increase the ionic radii of substituted metals where r(Fe^{3+}), r(Zn^{2+}), r(Cu^{2+}) ,and r(Mn^{2+}) r(Co^{2+}) are taken as: (tetra: 0.49 and octa:0.645 Å), (tetra.: 0.60 and octa:0.74 Å), (tetra.: 0.57 and oct.:0.73 Å), (tetra: 0.58 and octa: 0.72Å) and (tetra: 0.58 and octa: 0.745 Å), respectively taking into consideration the corresponding cation distribution [39].

Accordingly, the shared and unshared edges also increase with replaced Co^{2+} by Zn^{2+}, Cu^{2+} and Mn^{2+} ions in spinel ferrite NPs [40, 41].

The theoretical lattice parameter a_{the} is also calculated using the relation given below[42];

$$a_{the.} = \frac{8}{3\sqrt{3}}\left[(r_A + R_0) + \sqrt{3}(r_B + R_0)\right] \qquad (5)$$

Table 1 depicts the theoretical and experimentally lattice parameter for each composition. From this figure it can be seen that the variation of theoretical values of lattice constant for $M_xCo_{1-x}Fe_2O_4$ NPs is approximated to experimentally lattice parameter values [43].

3.1.2. Fourier Transform Infrared Spectrometer (FTIR)

FTIR was a helpful method that receives information concerning chemical functional groups equaling to the synthesized ferrites.

Figure 2 displays the FTIR spectra of $M_xCo_{1-x}Fe_2O_4$ NPs. The curves include absorption peaks at 420, 584, 600, 1136, 1629, and 2344 cm^{-1}. Existence of the two active absorption bands$v_1 and v_2$ in the FTIR spectra confirms the cubic spinel structure of the ferrite NPs. The higher frequency band

$\upsilon_1$and lower frequency band $\upsilon_2$were attributed to the stretching vibration of the tetrahedral A-site and the octahedral B-site [44-47]. The values of $\upsilon_1 and \upsilon_2$ are listed in Table (S2).

…… **Figure (2)** ……..

The force constant of atoms at tetrahedral and octahedral sites was defined by the following relations [48].

The variation of F_t and F_o for each composition for $M_xCo_{1-x}Fe_2O_4$ ferrite NPs is illustrated in (Fig. S3). It can be seen that $F_t > F_o$, which is attributed to the shorter bond length of the A-site compared to bond length of the B-site, where the relation between the bond length and force constant is an inverse proportionality[49, 50].

Debye temperature θ_D can be specified through the FTIR bands [50]. Figure (S4) presents the behavior of Debye temperature θ_D for the composition of ferrite NPs which it displayed that θ_D lies in the range of 681.52–708.87 K [51]. The Debye temperature and force constant at tetrahedral and octahedral sites are presented in Table (S2).

3.1.3 Scanning Electron Microscopy (SEM):

The uniform particles distribution and the morphology of $M_xCo_{1-x}Fe_2O_4$ (M= Zn, Cu, and Mn) ferrite NPs are presented in figure 3. It can be seen that the grain size and shape are significantly affected by the substitution of metals on CFO NPs with the existence of soft agglomeration [52-54].

…… **Figure (3)** ……...

3.1.4 Energy Dispersive of X-ray (EDs) Spectroscopy and elemental mapping images

Figure 4 presents the EDS measurements for $M_xCo_{1-x}Fe_2O_4$ NPs which indicate, the grown NPs are stoichiometric and homogeneous with a uniform distribution. For CFO NPs, the EDS micrographs confirmed the existence of Fe, Co, C and O without the presence of any signature of substituted metals. The EDS analysis for $M_xCo_{1-x}Fe_2O_4$ NPs confirmed no impurity elements were found in the synthesized samples NPs except for ZCFO NPs where found of sulfur ion may attributed to existence residue of sulfate group [55].

…… **Figure (4)**……

The elemental mapping images of ZCFO NPs are shown in figure (S5). The images are labeled as C K, Co K, Fe K, Zn K, and O K for ZCFO NPs. From this figure it is clear that the ZCFO NPs are homogeneous in terms of distribution of C, Co, Fe, Zn, and O atoms in the base ferrite NPs [56].

3.2. Electrochemical performance of ANDH on adjusted SPE electrode

The voltammetric performance of ANDH at SPE was studied utilizing cycle voltammetry (Fig. 5A). On the other hand, its represent just one oxidation peak, outwardly reduction signal peak witnessed at opposite scan; meaning that oxidation of ANDH is an irreversible manner at various electrodes (carbon SPE, modified SPE with CFO, ZCFO, CCFO, and MCFO NPs) in the likely range from 550 to 1050 mV in 0.04 M BR buffer pH 7.0, at scan rate 100 mVs^{-1}. For illustration ideas, CV was practiced, the SPE adjusted with the ZCFO NPs presented raised the current strength and downshift for limited positive potentials (E=0.895V) for the voltammetric oxidation of ANDH, (10 $mmolL^{-1}$), comparing with non-modified or modified with other ferrite NPs at all electrolyte pH value.

The turn for less positive potentials received by the SPE modified ZCFO NPs (E= 0.895 V), as distinguished with the bare SPE (E=0.910 V) and other ferrite modified system indicates an energy band gaps of spherical NPs ZCFO NPs (3.37V) [57], and the spongy porous agglomerate created from the ZCFO NPs sequestration at the electrode surface should play a large porous area[58]. Moreover synergistic character attached to ZCFO NPs and carbon[59], stimulating the electron variation at the electrode covering suspension interface thus improving the voltammograms signals [60, 61].

3.2.1. Optimization of experimental requirements.

A qualified research of screen-printed electrodes printed on-site provided with and without the aid of a ferrite NPs mediator for measuring 5µg/ml ANDH that displayed in Fig. (5B). Strong-defined and distinctive ANDH oxidation signals were received applying the considered electrodes. In our study, the experimental parameters effect such as electrolyte pH, scan rate and modifier were studied and optimized. The height of anodic peak current response was used to assess the influence of the factors.

……. Figure (5A&B) …….....

3.2.2. Effect of Solution pH

The pH influence was considered in the range among 5.0 and 10.0 to enhance the voltammetric response. Figure (S6) represents the voltammetric oxidation of ANDH through 0.04 M BR electrolyte buffer at varying pH range. It is clear that the peak current drops as the pH conditions rise above 7.0 or decline 6.0 because of the dissociation constant (pKa) values of ANDH which is 4.91 [62].

Consequently, besides a qualified knowledge of screen-printed electrodes printed on-site (made with and without the use of a ferrite NPs modifier) for measuring 5µg/ml, ANDH is given a well-defined and clear ANDH oxidation signals and were received applying the studied electrodes. The comparison of the anodic peak current values at distinct pH values of the carbon screen-printed electrode with CCFO, ZCFO, CCFO, and MCFO NPs was shown in figure (S6). Its exhibits great anodic current for ANDH than bare Carbon SPE, due to the adequate ionic conductivity, inclusive electrochemical gaps of ferrite plus the pre-absorption impact of ferrites. This pointer to the redox response of the charging current, improvements occurred low exposure limit and responsiveness. It is remarked that the peak potential changes to less positive with the increase in pH value following the equation:

$$E(V) = 1.3215 - 0.0587\text{pH} \quad (\text{R} = 0.9964) \qquad (6)$$

The linearity was demonstrated in pH range 5.0–10.0, followed by the slope of -0.0587 V/pH. The slope value of the relationship is really close to that demanded Nernstian value of -0.059 V [63], point near the protons associate in the electrode redox method, which the voltammetric method including the equivalent amount of protons and electrons, and that the electro-oxidation of ANDH is a pH-dependent manner.

3.2.3. Square-wave voltammetry parameters:

Once adjusted SPE electrode with ZCFO NPs (FZSPE) are applied, the value variation of f has a complicated importance impact on Ip, created by this alternative matches to the immediate variation of both factors x and y, where in$x = \kappa f^{-1/2}$, $y = \text{r}f^{-1/2}$,k is a constant notice to various charge transference rate constant (k_s)) by $\kappa = k_s D^{-1/2}$,D is the diffusion coefficient and r is the radius of the electrode[64].

Founded on that, the *f* effect on *Ip* and *Ep* was studied from 10 to 120 s^{-1}. Thus, the significant voltammograms revealed that the rise in f produced from an improvement in *I.* As shown in figure (S7), *Ip* extended linearly with the increasing of *f* until 50s^{-1}, and beyond this, the peak flow approximately constant values.

Recognizing the highest existence at 50 s^{-1}, a characteristic profile that takes place in an unchangeable redox method controlled with adsorption. Consistent with SWV method involving spherical electrodes, *Ep* has the linear relation with log (*f*), through the slope:

$$\frac{\Delta E_p}{\Delta \log(f)} = \frac{-2.3\ RT}{\alpha n F} \qquad (7)$$

where T is the temperature, R is the gas constant,α is the electron transfer coefficient, n is the number of electrons, and F is the Faraday constant [64].

Consequently, for ANDH oxidation, there is a linear relationship among *Ep* with the log (*f*), when the plot of Δlog (*f*) vs ΔEp resulted in a straight-line curve given by equation [65]:

$$E_p = 0.0551 \log(f) + 0.8557 \quad , \quad (R^2) = 0.9935 \qquad (8)$$

Upon the over relation examine the α=0.5 and replacing the traditional values of T, R, and F into the above equation between *Ep* and log (*f*), the calculated n value as approximately equivalent to ≈2, conceding for the measurement step of the redox method.

The ANDH composition is very multifaceted because of its conjugated double bonds in the chemical formation, eliminating and donor groups of electrons and steric hindrance that drives suggested mechanism hard to obvious conferred. Evaluating the fragments showing the most likely position of oxidation at the amino group which includes loan pair of electrons besides rings is

more unprotected and subjected to displayed reaction, registering the most feasible place of oxidation on the electrode outside as presented in figure 6.

……..…….Figure (6) ……..……..

3.2.4. Calibration Curve:

All the previous factors were examined not only to construct the analytical curves for the ANDH oxidation means at FZSPE in 0.04 M BR, but also to optimize the sensitivity of the recommended methodology and for employment in quality control for pharmaceutical formulations and spiked urine. Linear calibration curves produced from continuous raises a set suitable concentration of the stock ANDH solution into the voltammetric cell with volume improved to 5.0 ml of the 0.04M BR buffer (pH 7.0). The charge density appeared from SWV responses were associated with ANDH concentration range from 0.64 µg/ml to 8.18 µg/ml of ANDH, where the results presented a relational development in Ip with the ANDH concentration, with a small turn in Ep, declaring strong adsorption of reactants and reagents of the redox method at the exterior of electrode, as displayed in figure 7. In this calibration means, three repeated times for analytical curves were estimated, and the results presented, serve an average of the all resulted from curves. The correlation of analytical curves for ANDH oxidation at FZSPE can consequently designate by an equation:

$$\text{Current density}\left(\frac{\mu A}{cm^2}\right) = 0.27\ C\left(\frac{\mu g}{ml}\right) + 0.9958 \quad (R^2 = 0.9986)\ (9)$$

Consequently, to estimate the existence of random errors was considered by a consequence test to check if the variance within the intercepts produced in these analytical curves and the standard values generated from random error.

…… **Figure (7)** ……..……..

Furthermore, the quantification limit (QL) and detection limit (DL) for ANDH oxidation at FZSPE, consulting to before optimized SWV parameters, were measured take on the criteria given in the test above. Further important parameter examined in this study was the reproducibility of the voltammetric system, which was evaluated in three various stock solutions including 5.5 µgm/ml of ANDH, and the RSD value produced for n=3 was less than 1.1%. Moreover, the repeatability was also evaluated in the corresponding solution as above and the RSD issued for n=3 was close to being 1.16 %.

As shown from table (S3), the closeness of analysis proceeds received for DL and QL by via SWV at FZSPE, and HPLC methods, it can be remarked that the application of FZSPE with the SWV method implementing an strong, helpful, easy and low-cost analytical approach for measurement of ANDH due to the circumstances of its practicing in the simple and reliable analysis in concentrations connecting that performed by HPLC, which is a lot of the standard system employed in investigation of drug mixture.

Table (S4) records comparison of the carbon SPE and modified SPE for the measurement of ANDH with the related processes. Our work demonstrated the lowest DL comparing other values stated in the literature survey using another method.

3.2.5. Accuracy:

To determine the efficiency of the suggested approach, the results of the ANDH assay in pure form imposed by the expected voltammetric method was associated with those achieved utilizing the reference HPLC technique for the described purpose. Statistical comparison of the results received by the SWV way and those concerned with the reported HPLC process via Student's t-test and

change ratio F-test demonstrated no notable variation within the two procedures as exhibited in table (S5).

3.3. Application of SWV analytical methodology in pharmaceutical samples:

SWV analytical approach presented earlier was accepted to the quantitative interpretation of ANDH in pharmaceuticals usage. The results and improvements of observed concentrations of ANDH added to pharmaceutical mixtures are delivered in table (S6) for tablets. No oxidation reagents and no further noise or peaks existent in several estimations occurred in the measured potential area in the analytical peak position. The efficiency of the voltammetric system was defined by its return through spiked investigations. The results confirm the efficacy of the recommended methods for the quantification of ANDH in tablets. Those results exhibit that, both SWV methods had sufficient efficiency and accuracy which consequently can be related to the determination of ANDH in pharmaceuticals without any interference.

3.4. Analysis of real sample:

Validation of the suggested design for the quantitatively of the ANDH was studied in 0.04M BR buffer pH 7.0, at FZSPE, with f=50 s^{-1}, a=30 mV, ΔEs= 2 mV.

The resulted curve showed a straight line in the linear range 0.5 µg/ml to 8.2 µg/ml with regression coefficient, R= 0.999, the LOD is 0.8 µg/ml. From the calibration curve, four various concentrations are taken to be examined five times to determine the accuracy and accuracy of the proposed technique that is shown in table (S7).

SWV technique was also used to quantification of ANDH in the spiked sample of human serum. Plasma return was measured through serum-free drugs with identified quantities of ANDH. Quantitative detection was achieved, by adding a probate known concentration of the standard

drug solution in the plasma sample that was strongly determined. Table (S8) shows the determination results received for three plasma samples with recovery, sequencing, and RSD.

3.5. Antimicrobial activity of ZCFO NPs.

For the first time, ZCFO NPs (1000ppm) displayed a promising and successful effect as antibacterial against multi-drug resistant bacteria, including the high activity upon both *E. coli* and *E. faecalis* (27.0 mm ZOI) as shown in figure (8A) (*E. faecalis*).

Figure (8A) displayed the effect of ZCFO NPs on *E. faecalis* and represented the 3D image of ZOI around the ZCFO NPs disk. The yellowish green color represented the growth of bacterial cells, while the faint blue area investigated the bactericidal effect of ZCFO NPs upon *E. faecalis.*

On the other hand, ZCFO NPs showed a maximal growth inhibition towards the standard ATTC bacteria like *K. pneumoniae* (28.0 mm ZOI), as shown in figure (8B) followed by *P. aeruginosa* (27.0 mm ZOI).

Figure (8B) represented the activity of ZCFO NPs on *K. pneumoniae*and explained the 3D image of ZOI around the ZCFO NPs disk. The violet color represented the growth of bacterial cells, while the faint green area investigated the bactericidal effect of ZCFO NPs upon *K. pneumoniae.*

……**Figure (8 A&B)**…….……

Additionally ZCFONPs (new smart antifungal agent) active against *C. albicans* (the common urinary and vaginal pathogen) that, produced 18.0 mm ZOI while, the standard antibiotic (NS; 100µg/ml) inactive against it. Additionally, all tested microbes were resistant to the solvent (DMSO) used in ferriteNPs solubility as presented in table (2).

…..……...…..……Table (2)…….……..….

The width of inhibition zone represents the importance of sensitivity of pathogens. Clearly, in standard ATCC bacteria, Gram-negative bacteria showed a higher inhibition zone than Gram-positive bacteria. It was means; Gram-negative bacteria were more sensitive to ZCFO NPs associated with the Gram-positive bacteria in ATTC standard strains. The same purpose of antimicrobial activity has been kept with CuONPs, and ZnONPs [66].

On the other hand, in case of multidrug-resistant bacteria, ZCFO NPs active against both Gram-positive and Gram-negative equally. On the contrary, AgNPs have been reported to perform a modified form of antimicrobial action upon Gram-negative and Gram-positive bacteria [32].

In our results, we should offer compelling proof of the efficacy of ZCFO NPs (1000 ppm), to hinder and reduce the infections of urinary tract and blood samples against, multidrug resistant bacteria, and unicellular pathogenic fungi. ZCFO NPs capacity to restrain bacterial and fungal extension was promising and greater than standard antibiotics used in our experiment.

Similar reports and comparative studieswere described the role of metals substituted CFO NPs as antibacterial agents against pathogenic bacteria. Gingasu *et al*. [67] noted the action of CFO and silver CFO NPs (10 mg/mL, for both) on *E. coli*, *P. aeruginosa*, *S. aureus*, *E. faecalis*, *B. subtilis* and *C. albicans* ZOI about 8.0, 6.0, 6.0, 10.0, 8.0, and 6.0 mm respectively.

Furthermore, Mohammed *et al*, [68] were described the performance of silver CFO NPs (1.0 mg/ml) that, synthesized by sol-gel method as antibacterial agent repressed the growth of *E. coli* by 15.0 mm ZOI, and *S. aureus* by 12.0 mm ZOI.

There are various reaction mechanisms for the antibacterial action of ZCFO NPs [69]. Investigations revealed that zinc attaches to the membranes of microbes, related to mammalian

cells, increasing the lag stage of the growth period and raising the production rate of the microbes so, to complete cell division, more times had been consumed [70].

The different hypothesis stated that, the principal chemical kinds providing to the experience of the antibacterial activity were considered to be powerful oxides; for example, super-oxide (O_2^-), and hydrogen peroxide (H_2O_2) produced from ZCFO NPs surface [71].

These quick oxides immediately enter the cell wall of bacteria and produce cell damage. The diffusion speed of active oxides within the bacteria cell wall performs an essential part in the inhibition speed of ZCFO NPs toward bacteria. The investigations showed that active oxides produced from transition metals-substituted CFO NPs own more ability to insert the cell wall and reduce the cell division of Gram-negative bacteria rather than Gram-positive bacteria [70]. The exact mechanism of interaction among bacteria and transition metal-substituted CFO NPs requires more examinations.

The advantages of inorganic NPs are their high surface-to-volume degrees, numerous structural deficiencies, several organizations, and their nano-scale range, that contributes more effective points to connect with fungi, bacteria, and viruses. This is the significant difference within NPs and the general organic antimicrobial agents and could overcome the risk of advancing antimicrobial defense [72].

Finally, our results present a novel, effective, low cost, promising biosensors, and broad-spectrum antimicrobial agents. ZCFO NPs would be applied in medical and pharmaceutical applications, surface disinfectant, hospitals paints, labs, dental supplements, pediatric and geriatric clinics.

Conclusion

Metals doped CFO NPs were synthesized by eco-friendly and cost-effective sol-gel technique. XRD and FTIR data indicated the presence of cubic spinel phase. The new disposable SPE have several benefits of mass production, reproducibility of the production procedure, quite simple, sheep and quick education technique as well as capability for creation working and reference electrodes which give the opportunity of measurements on small volumes with high reproducibility. All of the SPEs sensors have high mechanical sturdiness and accurate adherent to the PVC substrate. The results obtained in the present study display that, the SPEs can successfully be applied in the SWV of ANDH using the procedures approved in the application in quality control in productions of ANDH, pharmaceutical formula and biological flutes comparing with official methods. On the other hand, ZCFO NPs were smart antimicrobial agents active against multidrug resistant pathogens that give the superior applications in the infectious diseases control.

Acknowledgments:

The authors would like to thank the Nanotechnology Research Unit (**P.I. Prof. Dr. Ahmed I. El-Batal**), Drug Microbiology Lab., Drug Radiation Research Department, NCRRT, Egypt, for financing and supporting this study under the project "Nutraceuticals and Functional Foods Production by using Nano/ Biotechnological and Irradiation Processes". Also, the authors would like to thank **Dr. Mohamed Gobara (Ass. Prof. at Egyptian Military Technical Collage)**, **National Organization for Drug Control and Research (NODCAR),** and **Zeiss microscope** team in Cairo for their invaluable advice during this study

Compliance with Ethical Standards

Conflict of interest: The authors declare that they have no conflict of interest.

Ethical statement

This article does not contain any studies with human participants or animals performed by any of the authors.

References

[1] R. Bhattacharya, P. Mukherjee, Biological properties of "naked" metal nanoparticles, Advanced drug delivery reviews 60(11) (2008) 1289-1306.

[2] M. Dar, D. Varshney, Effect of d-block element Co2+ substitution on structural, Mössbauer and dielectric properties of spinel copper ferrites, Journal of Magnetism and Magnetic Materials 436 (2017) 101-112.

[3] A. Amirabadizadeh, Z. Salighe, R. Sarhaddi, Z. Lotfollahi, Synthesis of ferrofluids based on cobalt ferrite nanoparticles: Influence of reaction time on structural, morphological and magnetic properties, Journal of Magnetism and Magnetic Materials 434 (2017) 78-85.

[4] S.A. Pour, H.R. Shaterian, M. Afradi, A. Yazdani-Elah-Abadi, Carboxymethyl cellulose (CMC)-loaded Co-Cu doped manganese ferrite nanorods as a new dual-modal simultaneous contrast agent for magnetic resonance imaging and nanocarrier for drug delivery system, Journal of Magnetism and Magnetic Materials 438 (2017) 85-94.

[5] M.T. Farid, I. Ahmad, M. Kanwal, G. Murtaza, I. Ali, M.N. Ashiq, S.A. Khan, Magnetic and electric behavior of praseodymium substituted CuPryFe2-yO4 ferrites, Journal of Magnetism and Magnetic Materials 422 (2017) 337-343.

[6] O. Alcalá, S. Briceño, W. Brämer-Escamilla, P. Silva, Toroidal cores of MnxCo1−xFe2O4/PAA nanocomposites with potential applications in antennas, Materials Chemistry and Physics 192 (2017) 17-21.

[7] Z. Yan, J. Luo, Effects of CeZn co-substitution on structure, magnetic and microwave absorption properties of nickel ferrite nanoparticles, Journal of Alloys and Compounds 695 (2017) 1185-1195.

[8] R. Sharma, P. Thakur, P. Sharma, V. Sharma, Ferrimagnetic Ni2+ doped Mg-Zn spinel ferrite nanoparticles for high density information storage, Journal of Alloys and Compounds 704 (2017) 7-17.

[9] S. Winder, Power supplies for LED driving, Newnes 2016.

[10] P. Samoila, C. Cojocaru, L. Sacarescu, P.P. Dorneanu, A.-A. Domocos, A. Rotaru, Remarkable catalytic properties of rare-earth doped nickel ferrites synthesized by sol-gel auto-combustion with maleic acid as fuel for CWPO of dyes, Applied Catalysis B: Environmental 202 (2017) 21-32.

[11] X. Niu, B. Zong, H. Hu, B. Wu, Influence of Sn4+-substituted on the magnetic properties and power loss of Ni-Zn soft magnetic ferrites, Optik-International Journal for Light and Electron Optics 134 (2017) 135-139.

[12] M. Anupama, B. Rudraswamy, N. Dhananjaya, Investigation on impedance response and dielectric relaxation of Ni-Zn ferrites prepared by self-combustion technique, Journal of Alloys and Compounds 706 (2017) 554-561.

[13] H. El Moussaoui, T. Mahfoud, S. Habouti, K. El Maalam, M.B. Ali, M. Hamedoun, O. Mounkachi, R. Masrour, E. Hlil, A. Benyoussef, Synthesis and magnetic properties of tin spinel ferrites doped manganese, Journal of Magnetism and Magnetic Materials 405 (2016) 181-186.

[14] S. Patil, A. Pawar, S. Tilekar, B. Ladgaonkar, Investigation of magnesium substituted nano particle zinc ferrites for relative humidity sensors, Sensors and Actuators A: Physical 244 (2016) 35-43.

[15] E. El-Ghazzawy, M. Amer, Structural, elastic and magnetic studies of the as-synthesized Co1− xSrxFe2O4 nanoparticles, Journal of Alloys and Compounds 690 (2017) 293-303.

[16] S. Algude, S. Patange, S.E. Shirsath, D. Mane, K. Jadhav, Elastic behaviour of Cr3+ substituted Co–Zn ferrites, Journal of Magnetism and Magnetic Materials 350 (2014) 39-41.

[17] M. Raghasudha, D. Ravinder, P. Veerasomaiah, K. Jadhav, M. Hashim, P. Bhatt, S.S. Meena, Electrical resistivity and Mössbauer studies of Cr substituted Co nano ferrites, Journal of Alloys and Compounds 694 (2017) 366-374.

[18] T.A. Rocha-Santos, Sensors and biosensors based on magnetic nanoparticles, TrAC Trends in Analytical Chemistry 62 (2014) 28-36.

[19] L. Su, W. Qin, H. Zhang, Z.U. Rahman, C. Ren, S. Ma, X. Chen, The peroxidase/catalase-like activities of MFe2O4 (M= Mg, Ni, Cu) MNPs and their application in colorimetric biosensing of glucose, Biosensors and Bioelectronics 63 (2015) 384-391.

[20] S. Negahban, M. Fouladgar, G. Amiri, Improve the performance of carbon paste electrodes for determination of dobutamine using MnZnFe2O4 nanoparticles and ionic liquid, Journal of the Taiwan Institute of Chemical Engineers 78 (2017) 51-55.

[21] Z. Zhu, R. Gonthier, L. Neirinck, High-performance liquid chromatography–mass spectrometry method for determination of anagrelide in human plasma, Journal of Chromatography B 822(1-2) (2005) 238-243.

[22] H.T.S. Britton, R.A. Robinson, LXI.—The use of the antimony–antimonous oxide electrode in the determination of the concentration of hydrogen ions and in potenliometric titrations. The Prideaux–Ward universal buffer mixture, Journal of the Chemical Society (Resumed) (1931) 458-473.

[23] H.M. Elqudaby, H.A. Hendawy, E.R. Souaya, G.G. Mohamed, G.M. Eldin, Utility of activated glassy carbon and pencil graphite electrodes for voltammetric determination of nalbuphine hydrochloride in pharmaceutical and biological fluids, International Journal of Electrochemistry 2016 (2016).

[24] J.T. Seil, T.J. Webster, Antimicrobial applications of nanotechnology: methods and literature, International journal of nanomedicine 7 (2012) 2767.

[25] A. Ashour, A.I. El-Batal, M.A. Maksoud, G.S. El-Sayyad, S. Labib, E. Abdeltwab, M. El-Okr, Antimicrobial activity of metal-substituted cobalt ferrite nanoparticles synthesized by sol–gel technique, Particuology, In Press, (2018).

[26] A.A. Reheem, M.A. Maksoud, A. Ashour, Surface modification and metallization of polycarbonate using low energy ion beam, Radiation Physics and Chemistry 125 (2016) 171-175.

[27] A.A. Reheem, A. Atta, M.A. Maksoud, Low energy ion beam induced changes in structural and thermal properties of polycarbonate, Radiation Physics and Chemistry 127 (2016) 269-275.

[28] A.I. El-Batal, G.S. El-Sayyad, A. El-Ghamry, K.M. Agaypi, M.A. Elsayed, M. Gobara, Melanin-gamma rays assistants for bismuth oxide nanoparticles synthesis at room temperature for enhancing antimicrobial, and photocatalytic activity, Journal of Photochemistry and Photobiology B: Biology 173 (2017) 120-139.

[29] A.I. El-Batal, G.S. El-Sayyad, A. El-Ghamery, M. Gobara, Response surface methodology optimization of melanin production by *Streptomyces cyaneus* and synthesis of copper oxide nanoparticles using gamma radiation, Journal of Cluster Science 28(3) (2017) 1083-1112.

[30] A.I. El-Batal, N.E. Al-Hazmi, F.M. Mosallam, G.S. El-Sayyad, Biogenic synthesis of copper nanoparticles by natural polysaccharides and *Pleurotus ostreatus* fermented fenugreek using gamma rays with antioxidant and antimicrobial potential towards some wound pathogens, Microbial pathogenesis 118 (2018) 159-169.

[31] G. Funke, D. Monnet, A. von Graevenitz, J. Freney, Evaluation of the VITEK 2 system for rapid identification of medically relevant gram-negative rods, Journal of clinical microbiology 36(7) (1998) 1948-1952.

[32] A. Baraka, S. Dickson, M. Gobara, G.S. El-Sayyad, M. Zorainy, M.I. Awaad, H. Hatem, M.M. Kotb, A. Tawfic, Synthesis of silver nanoparticles using natural pigments extracted from Alfalfa leaves and its use for antimicrobial activity, Chemical Papers 71(11) (2017) 2271-2281.

[33] H. El Moussaoui, T. Mahfoud, M.B. Ali, Z. Mahhouti, R. Masrour, M. Hamedoun, E. Hlil, A. Benyoussef, Experimental studies of neodymium ferrites doped with three different transition metals, Materials Letters 171 (2016) 142-145.

[34] S. Singhal, J. Singh, S. Barthwal, K. Chandra, Preparation and characterization of nanosize nickel-substituted cobalt ferrites (Co1− xNixFe2O4), Journal of Solid State Chemistry 178(10) (2005) 3183-3189.

[35] M.N. Akhtar, A.B. Sulong, M. Ahmad, M.A. Khan, A. Ali, M. Islam, Impacts of Gd–Ce on the structural, morphological and magnetic properties of garnet nanocrystalline ferrites synthesized via sol–gel route, Journal of Alloys and Compounds 660 (2016) 486-495.

[36] M. Hashim, S.E. Shirsath, S. Kumar, R. Kumar, A.S. Roy, J. Shah, R. Kotnala, Preparation and characterization chemistry of nano-crystalline Ni–Cu–Zn ferrite, Journal of Alloys and Compounds 549 (2013) 348-357.

[37] M.N. Akhtar, M.A. Khan, M. Ahmad, M. Nazir, M. Imran, A. Ali, A. Sattar, G. Murtaza, Evaluation of structural, morphological and magnetic properties of CuZnNi (CuxZn0. 5− xNi0. 5Fe2O4) nanocrystalline ferrites for core, switching and MLCI's applications, Journal of Magnetism and Magnetic Materials 421 (2017) 260-268.

[38] D. Venkatesh, G. Himavathi, K. Ramesh, Structural, magnetic, and electrical properties of Ni0. 65Zn0. 35− xCuxFe2O4 nanoferrite system, Journal of Superconductivity and Novel Magnetism 28(9) (2015) 2801-2807.

[39] L.-Z. Li, X.-X. Zhong, R. Wang, X.-Q. Tu, L. Peng, Structural and magnetic properties of Co-substituted NiCu ferrite nanopowders, Journal of Magnetism and Magnetic Materials 433 (2017) 98-103.

[40] K.M. Batoo, G. Kumar, Y. Yang, Y. Al-Douri, M. Singh, R.B. Jotania, A. Imran, Structural, morphological and electrical properties of Cd2+ doped MgFe2-xO4 ferrite nanoparticles, Journal of Alloys and Compounds 726 (2017) 179-186.

[41] J. Jadhav, S. Biswas, A. Yadav, S. Jha, D. Bhattacharyya, Structural and magnetic properties of nanocrystalline NiZn ferrites: In the context of cationic distribution, Journal of Alloys and Compounds 696 (2017) 28-41.

[42] R. Sharma, P. Thakur, M. Kumar, N. Thakur, N. Negi, P. Sharma, V. Sharma, Improvement in magnetic behaviour of cobalt doped magnesium zinc nano-ferrites via co-precipitation route, Journal of Alloys and Compounds 684 (2016) 569-581.

[43] R.D. Shannon, Revised effective ionic radii and systematic studies of interatomic distances in halides and chalcogenides, Acta crystallographica section A: crystal physics, diffraction, theoretical and general crystallography 32(5) (1976) 751-767.

[44] M. Amer, A. Matsuda, G. Kawamura, R. El-Shater, T. Meaz, F. Fakhry, Characterization and structural and magnetic studies of as-synthesized Fe2+ CrxFe (2− x) O4 nanoparticles, Journal of Magnetism and Magnetic Materials 439 (2017) 373-383.

[45] M. Amer, T. Meaz, A. Mostafa, H. El-Ghazally, Structural and physical properties of the nano-crystalline Al-substituted Cr–Cu ferrite, Journal of Magnetism and Magnetic Materials 343 (2013) 286-292.

[46] R. Kadam, S.T. Alone, M.L. Mane, A. Biradar, S.E. Shirsath, Phase evaluation of Li+ substituted CoFe2O4 nanoparticles, their characterizations and magnetic properties, Journal of Magnetism and Magnetic Materials 355 (2014) 70-75.

[47] A. Ghasemi, Compositional dependence of magnetization reversal mechanism, magnetic interaction and Curie temperature of Co1− xSrxFe2O4 spinel thin film, Journal of Alloys and Compounds 645 (2015) 467-477.

[48] S. Patange, S.E. Shirsath, K. Lohar, S. Algude, S. Kamble, N. Kulkarni, D. Mane, K. Jadhav, Infrared spectral and elastic moduli study of NiFe2− xCrxO4 nanocrystalline ferrites, Journal of Magnetism and Magnetic Materials 325 (2013) 107-111.

[49] M. Amer, Structural and magnetic studies of the Co1+ xTixFe2 (1− x) O4 ferrites, Journal of Magnetism and Magnetic Materials 426 (2017) 771-778.

[50] M. Amer, T. Meaz, S. Attalah, A. Ghoneim, Structural and magnetic characterization of the Mg0. 2− xSrxMn0. 8Fe2O4 nanoparticles, Journal of Magnetism and Magnetic Materials 363 (2014) 60-65.

[51] V. Cabuil, V. Dupuis, D. Talbot, S. Neveu, Ionic magnetic fluid based on cobalt ferrite nanoparticles: influence of hydrothermal treatment on the nanoparticle size, Journal of Magnetism and Magnetic Materials 323(10) (2011) 1238-1241.

[52] K.R. Babu, K.R. Rao, B.R. Babu, Cu2+-modified physical properties of Cobalt-Nickel ferrite, Journal of Magnetism and Magnetic Materials 434 (2017) 118-125.

[53] P. Chavan, L. Naik, P. Belavi, G. Chavan, R. Kotnala, Synthesis of Bi3+ substituted Ni-Cu ferrites and study of structural, electrical and magnetic properties, Journal of Alloys and Compounds 694 (2017) 607-612.

[54] Y. Köseoğlu, F. Alan, M. Tan, R. Yilgin, M. Öztürk, Low temperature hydrothermal synthesis and characterization of Mn doped cobalt ferrite nanoparticles, Ceramics International 38(5) (2012) 3625-3634.

[55] E.R. Kumar, P.S.P. Reddy, G.S. Devi, S. Sathiyaraj, Structural, dielectric and gas sensing behavior of Mn substituted spinel MFe2O4 (M= Zn, Cu, Ni, and Co) ferrite nanoparticles, Journal of Magnetism and Magnetic Materials 398 (2016) 281-288.

[56] M.T. Rahman, M. Vargas, C. Ramana, Structural characteristics, electrical conduction and dielectric properties of gadolinium substituted cobalt ferrite, Journal of Alloys and Compounds 617 (2014) 547-562.

[57] N. Kamarulzaman, M. Kasim, N. Chayed, Elucidation of the highest valence band and lowest conduction band shifts using XPS for ZnO and Zn0. 99Cu0. 01O band gap changes, Results in physics 6 (2016) 217-230.

[58] D. Kotsikau, M. Ivanovskaya, V. Pankov, Y. Fedotova, Structure and magnetic properties of manganese–zinc-ferrites prepared by spray pyrolysis method, Solid State Sciences 39 (2015) 69-73.

[59] R. Lucena, B. Simonet, S. Cárdenas, M. Valcárcel, Potential of nanoparticles in sample preparation, Journal of Chromatography A 1218(4) (2011) 620-637.

[60] H. Zhu, S. Zhang, Y.-X. Huang, L. Wu, S. Sun, Monodisperse M x Fe3–x O4 (M= Fe, Cu, Co, Mn) Nanoparticles and Their Electrocatalysis for Oxygen Reduction Reaction, Nano letters 13(6) (2013) 2947-2951.

[61] M. Eguílaz, R. Villalonga, P. Yáñez-Sedeño, J.M. Pingarrón, Designing electrochemical interfaces with functionalized magnetic nanoparticles and wrapped carbon nanotubes as platforms for the construction of high-performance bienzyme biosensors, Analytical chemistry 83(20) (2011) 7807-7814.

[62] H. Wan, A.G. Holmén, Y. Wang, W. Lindberg, M. Englund, M.B. Någård, R.A. Thompson, High-throughput screening of pKa values of pharmaceuticals by pressure-assisted capillary electrophoresis and mass spectrometry, Rapid communications in mass spectrometry 17(23) (2003) 2639-2648.

[63] E. Laviron, General expression of the linear potential sweep voltammogram in the case of diffusionless electrochemical systems, Journal of Electroanalytical Chemistry and Interfacial Electrochemistry 101(1) (1979) 19-28.

[64] Š. Komorsky-Lovrić, M. Lovrić, A. Bond, Square-wave voltammetry at spherical and disk microelectrodes as a function of electrode radius and frequency, Electroanalysis 5(1) (1993) 29-40.

[65] T.M. Oliveira, H. Becker, E. Longhinotti, D. De Souza, P. de Lima-Neto, A.N. Correia, Carbon-fibre microelectrodes coupled with square-wave voltammetry for the direct analysis of dimethomorph fungicide in natural waters, Microchemical Journal 109 (2013) 84-92.

[66] P. Kanmani, J.-W. Rhim, Properties and characterization of bionanocomposite films prepared with various biopolymers and ZnO nanoparticles, Carbohydrate polymers 106 (2014) 190-199.

[67] D. Gingasu, I. Mindru, L. Patron, J.M. Calderon-Moreno, O.C. Mocioiu, S. Preda, N. Stanica, S. Nita, N. Dobre, M. Popa, Green synthesis methods of CoFe2O4 and Ag-CoFe2O4 nanoparticles using hibiscus extracts and their antimicrobial potential, Journal of Nanomaterials 2016 (2016).

[68] S. Xavier, H. Cleetus, P. Nimila, S. Thankachan, R. Sebastian, E. Mohammed, Structural and antibacterial properties of silver substituted cobalt ferrite nanoparticles, Research Journal of Pharmaceutical, Biological and Chemical Sciences 5(5) (2014) 364-371.

[69] P.K. Stoimenov, R.L. Klinger, G.L. Marchin, K.J. Klabunde, Metal oxide nanoparticles as bactericidal agents, Langmuir 18(17) (2002) 6679-6686.

[70] L.L. Radke, B.L. Hahn, D.K. Wagner, P.G. Sohnle, Effect of abscess fluid supernatants on the kinetics of Candida albicans growth, Clinical immunology and immunopathology 73(3) (1994) 344-349.

[71] O. Yamamoto, J. Sawai, Preparation and characterization of novel activated carbons with antibacterial function, Bulletin of the Chemical Society of Japan 74(9) (2001) 1761-1765.

[72] R. Hernandez-Delgadillo, D. Velasco-Arias, J.J. Martinez-Sanmiguel, D. Diaz, I. Zumeta-Dube, K. Arevalo-Niño, C. Cabral-Romero, Bismuth oxide aqueous colloidal nanoparticles inhibit Candida albicans growth and biofilm formation, International journal of nanomedicine 8 (2013) 1645.

Table1: The average crystallite size, lattice parameters and inter-planar spacing of the unit cell calculated from XRD data of metals substituted nanocrystalline cobalt ferrites.

Table 2: Antibacterial and antifungal activity of ZCFO NPs synthesized by sol-gel methods against some standard strains (ATCC), multidrug-resistant bacteria, and unicellular fungi as ZOI (mm).

Table1: The average crystallite size, lattice parameters and inter-planar spacing of the unit cell calculated from XRD data of metals substituted nano-crystalline cobalt ferrites.

Doped Ferrites	FWHM β (degree)	inter-planar spacing d (Å)	Crystallite size D ±1.5 (nm)	Lattice parameter a_{exp} (Å)	Lattice parameter $a_{the.}$ (Å)
CFO	0.3026	2.52397	27.5600	8.3711	8.2370
ZCFO	0.6483	2.54522	12.8600	8.4415	8.3064
CCFO	0.5552	2.52826	15.0300	8.3853	8.2510
MCFO	0.2460	2.53712	33.9200	8.4147	8.2800

Table 2: Antibacterial and antifungal activity of ZCFO NPs synthesized by sol-gel methods against some standard strains (ATCC), multidrug-resistant bacteria, and unicellular fungi as ZOI (mm).

Microbial pathogens		**ZOI of ZCFO NPs (1000 ppm) (mm).**	**DMSO**	**AMC* and NS****
***Bacillus subtilis* ATCC 6633.**	**Standard strains (ATCC)**	$26.0^{de} \pm 0.76376$	▪ Negative.	Negative.
***Klebsiella pneumoniae* ATCC 4352.**		$28.0^{f} \pm 0.57735$	Negative.	Negative.
***Pseudomonas aeruginosa* ATCC 27853.**		$27.0^{ef} \pm 0.28868$	Negative.	Negative.
***Staphylococcus aureus* (MRSA).**	**Multidrug-resistant bacteria**	$26.0^{ef} \pm 1.00000$	Negative.	8.0 ± 1.00000
Staphylococcus epidermidis.		$25.0^{d} \pm 0.28868$	Negative.	Negative.
Acinetobacter baumannii.		$23.0^{c} \pm 0.57735$	Negative.	Negative.
Escherichia coli.		$27.0^{f} \pm 0.57735$	Negative.	Negative.
Enterococcus faecalis.		$27.0^{f} \pm 1.00000$	Negative.	10.0 ± 0.76376
Enterobacter cloacae.		$19.0^{b} \pm 1.00000$	Negative.	Negative.
***Candida albicans* ATCC 10231.**	**Unicellular Fungi**	$18.0^{a} \pm 1.15470$	Negative.	Negative.
LSD		1.33333	----------	----------

Values are means ± SD (n = 3). Data within the groups are analyzed using one-way analysis of variance (ANOVA) followed by $^{a, b, c, d, f}$ *Duncan's multiple range test (DMRT) at p<0.05.*

LSD = Least Significant Differences, ZCFO = Zinc Cobalt ferrites, DMSO = Dimethyl Sulphoxide.

- Negative means that no ZOI had been measured.

* AMC = Amoxicillin/Clavulanic Acid; 20/10 µg/ml (Antibacterial Standard).

** NS = Nystatin (Antifungal Standard).

Fig.1: XRD patterns of CFO, ZCFO, CCFO, and MCFO ferrite NPs as-obtained.

Fig.2: FTIR spectra of [A] CFO, [B] ZCFO, [C] CCFO and [D] MCFO ferrite NPs..

Fig. 3: SEM Images of [A] CFO, [B] ZCFO, [C] CCFO and [D] MCFO ferrite NPs..

Fig.4: EDs measurements for [A] CFO, [B] ZCFO, [C] CCFO and [D] MCFO ferrite NPs..

Fig.5: [A] Comparison between different SPD electrodes using the cyclic voltammograms of 5µgm/ml of ANDH in 0.04MB-R buffer pH 7.0 at scan rate 100 mVs^{-1} recorded at different working electrodes, [B] Comparison between different SPD electrodes in different 0.04 M BR buffer pH.

Fig.6: Illustration of proposed mechanism at screen printed electrode (SPE) with nano ferrite attached.

Fig.7: Square-wave voltammograms for DIM in 0.040 M B-R at pH 7.0 at FZSPE, with f=50 s^{-1}, a=30 mV, ΔEs=2 mV, and concentrations in the interval from 0.64µg/ml to 8.18µgm/ml of ANDH. Insert corresponds to the Analytical curves obtained from voltammograms.

Fig.8: Antibacterial activity of ZCFO NPs against A) *Enterococcus faecalis* and B) *Klebsiella pneumoniae* as ZOI.

HIGHLIGHTS

1- Synthesis and validation of spinel ferrite NPs using sol-gel technique.

2- The theoretical values of lattice constant for ferrite NPs are approximated to experimentally lattice parameter values.

3- The Debye temperature θ_D for the ferrite NPs composition lies in the range of 681.52 – 708.87 K.

4- ZCFO NPs posses a novel antimicrobial activity against selected MDR pathogens.

5- Improvement of a novel screen-printed sensor, modified with ZCFO NPs for rapid, sensitive and cost-effective quantification of ANDH present in the biological samples.

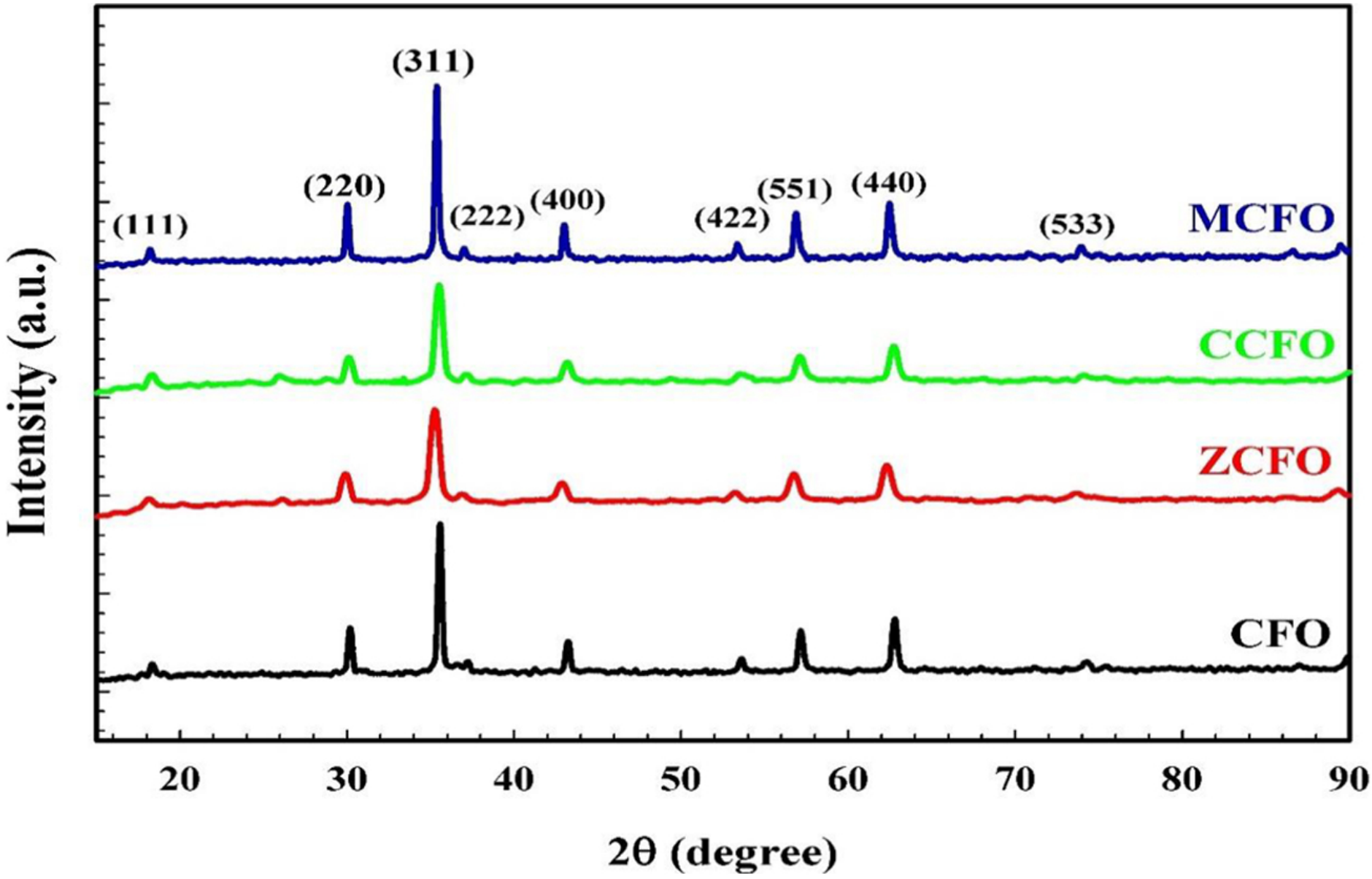
(311)
(220)
(111)
(222)
(400)
(422)
(551)
(440)
(533)
MCFO
CCFO
ZCFO
CFO
Intensity (a.u.)
20
30
40
50
60
70
80
90
2θ (degree)

Figure 1

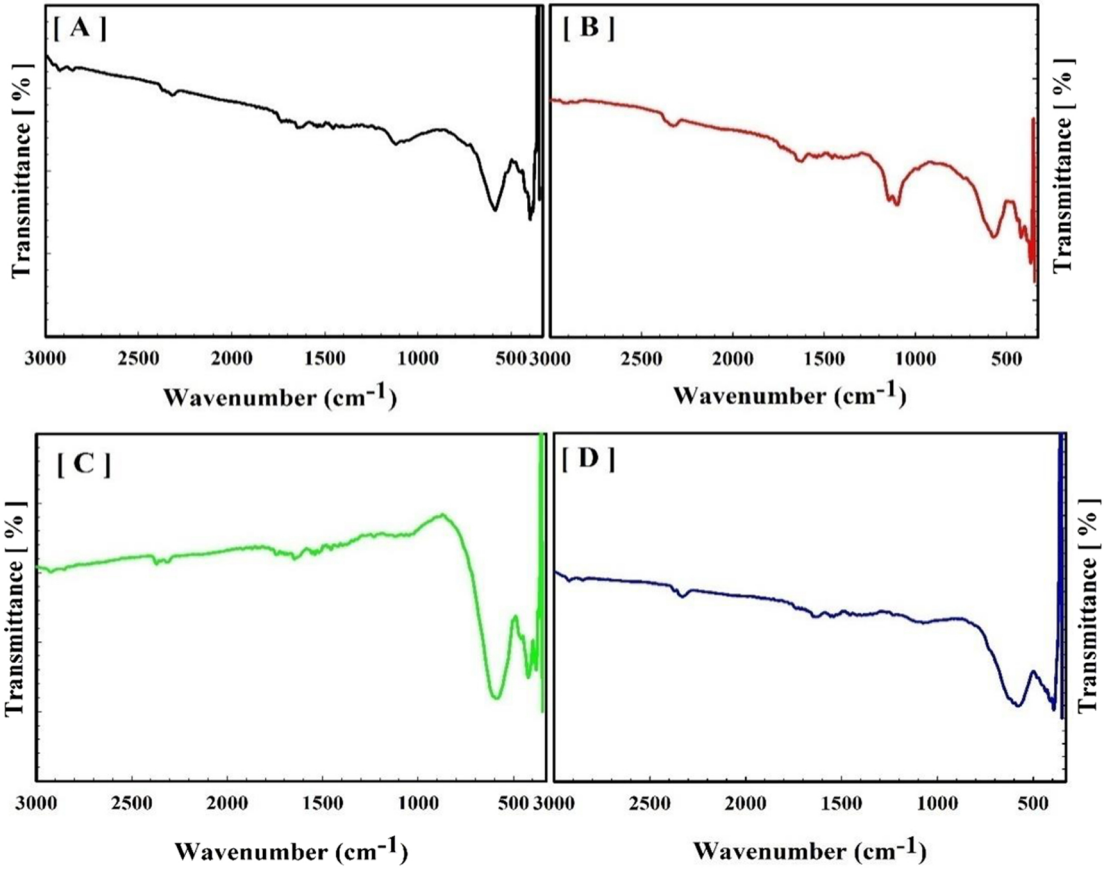
[A]
[B]
[C]
[D]
Transmittance [%]
Wavenumber (cm-1)
3000
2500
2000
1500
1000
500

Figure 2

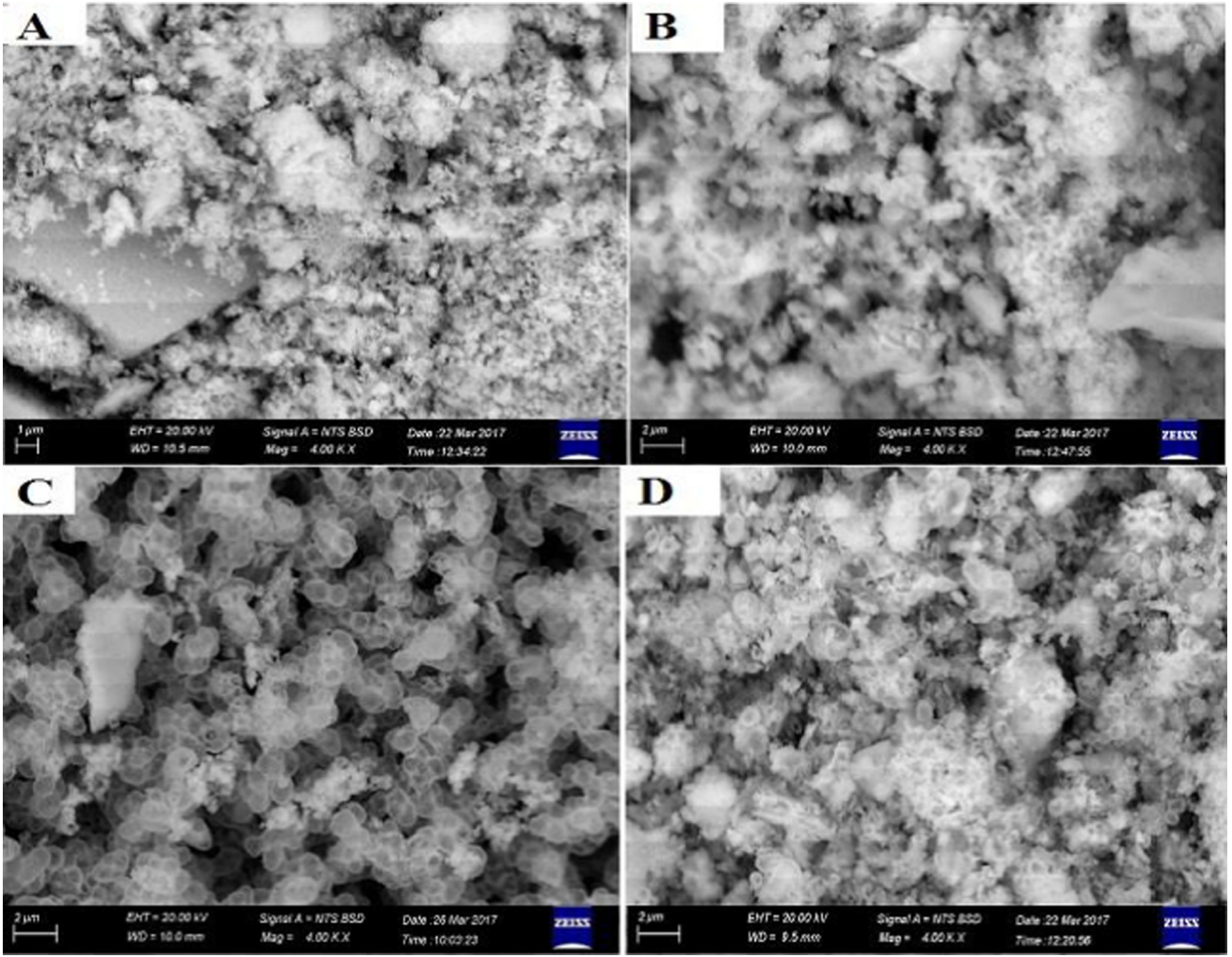
A
1 µm
EHT = 20.00 kV
WD = 10.5 mm
Signal A = NTS BSD
Mag = 4.00 K X
Date :22 Mar 2017
Time :12:34:22
B
2 µm
EHT = 20.00 kV
WD = 10.0 mm
Signal A = NTS BSD
Mag = 4.00 K X
Date :22 Mar 2017
Time :12:47:55
C
2 µm
EHT = 20.00 kV
WD = 10.0 mm
Signal A = NTS BSD
Mag = 4.00 K X
Date :26 Mar 2017
Time :10:03:23
D
2 µm
EHT = 20.00 kV
WD = 9.5 mm
Signal A = NTS BSD
Mag = 4.00 K X
Date :22 Mar 2017
Time :12:20:56

Figure 3

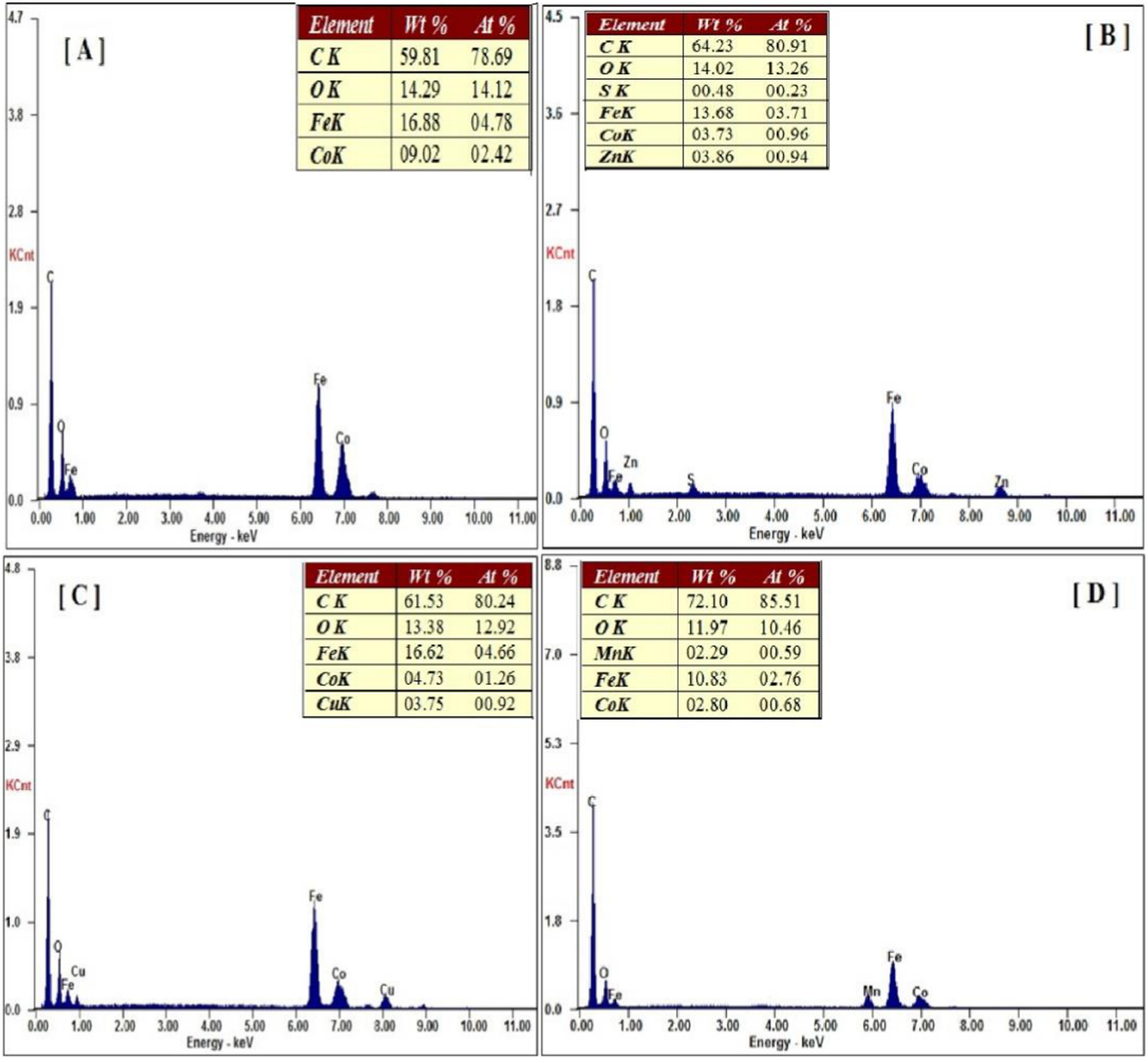
[A]
Element | Wt % | At %
C K | 59.81 | 78.69
O K | 14.29 | 14.12
FeK | 16.88 | 04.78
CoK | 09.02 | 02.42
KCnt
Energy - keV
[B]
Element | Wt % | At %
C K | 64.23 | 80.91
O K | 14.02 | 13.26
S K | 00.48 | 00.23
FeK | 13.68 | 03.71
CoK | 03.73 | 00.96
ZnK | 03.86 | 00.94
KCnt
Energy - keV
[C]
Element | Wt % | At %
C K | 61.53 | 80.24
O K | 13.38 | 12.92
FeK | 16.62 | 04.66
CoK | 04.73 | 01.26
CuK | 03.75 | 00.92
KCnt
Energy - keV
[D]
Element | Wt % | At %
C K | 72.10 | 85.51
O K | 11.97 | 10.46
MnK | 02.29 | 00.59
FeK | 10.83 | 02.76
CoK | 02.80 | 00.68
KCnt
Energy - keV

Figure 4

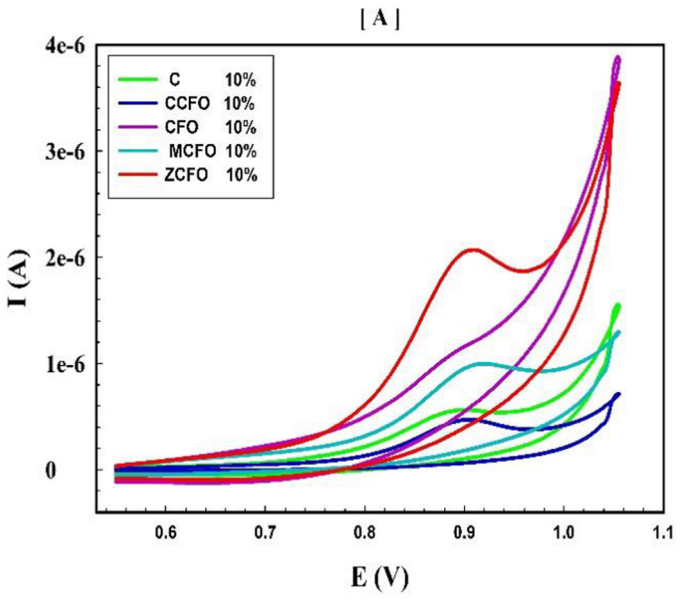
[A]
C 10%
CCFO 10%
CFO 10%
MCFO 10%
ZCFO 10%
I (A)
E (V)
4e-6
3e-6
2e-6
1e-6
0
0.6
0.7
0.8
0.9
1.0
1.1

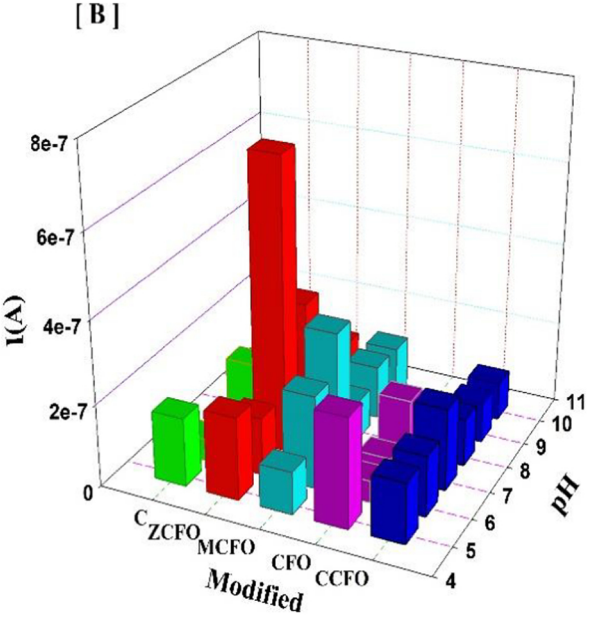
[B]
I(A)
8e-7
6e-7
4e-7
2e-7
0
C
ZCFO
MCFO
CFO
CCFO
Modified
pH
11
10
9
8
7
6
5
4

Figure 5

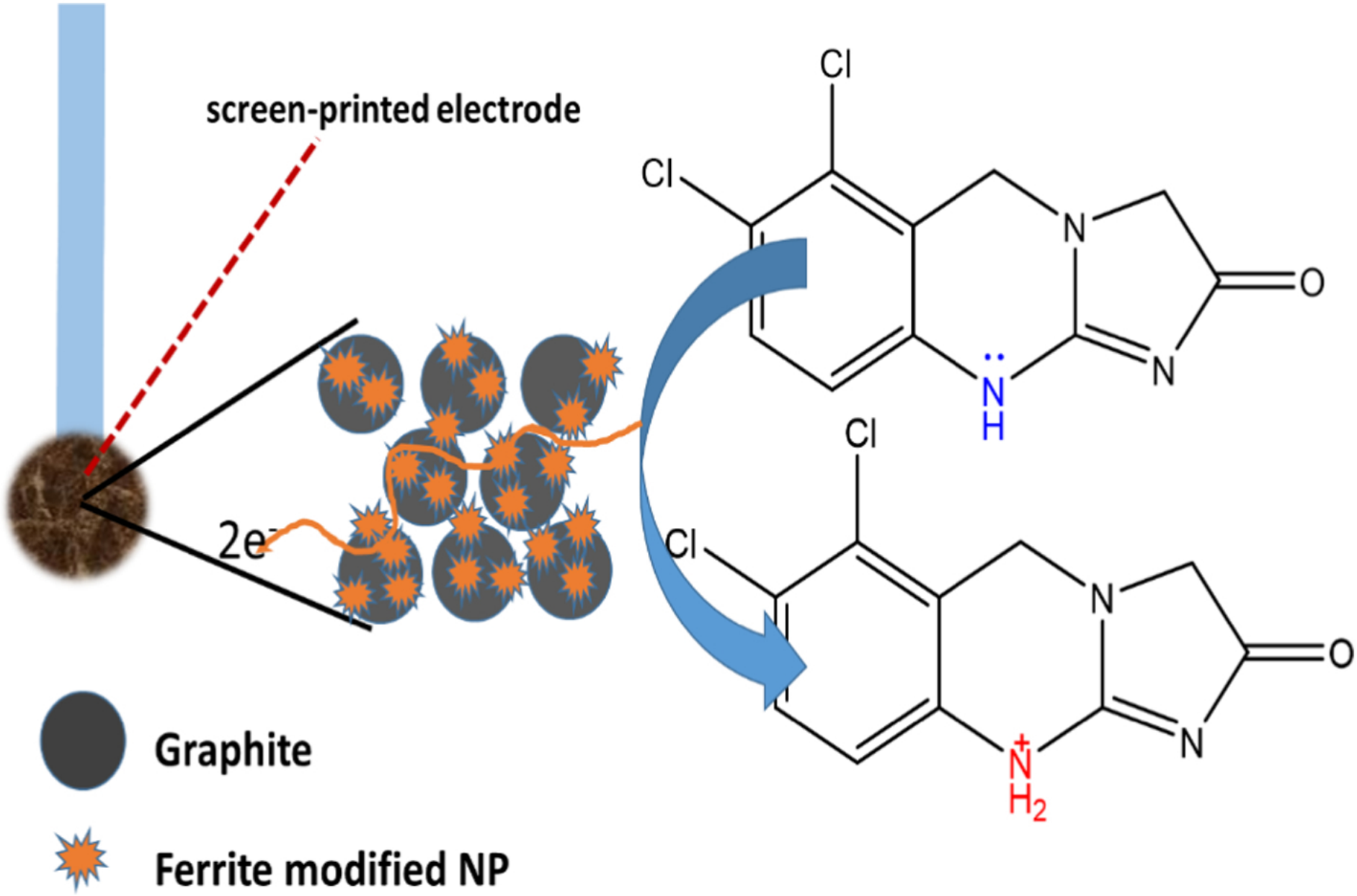
screen-printed electrode
2e⁻
Cl
Cl
N
O
N
N
H
Cl
Cl
N
O
N
N
H2
Graphite
Ferrite modified NP

Figure 6

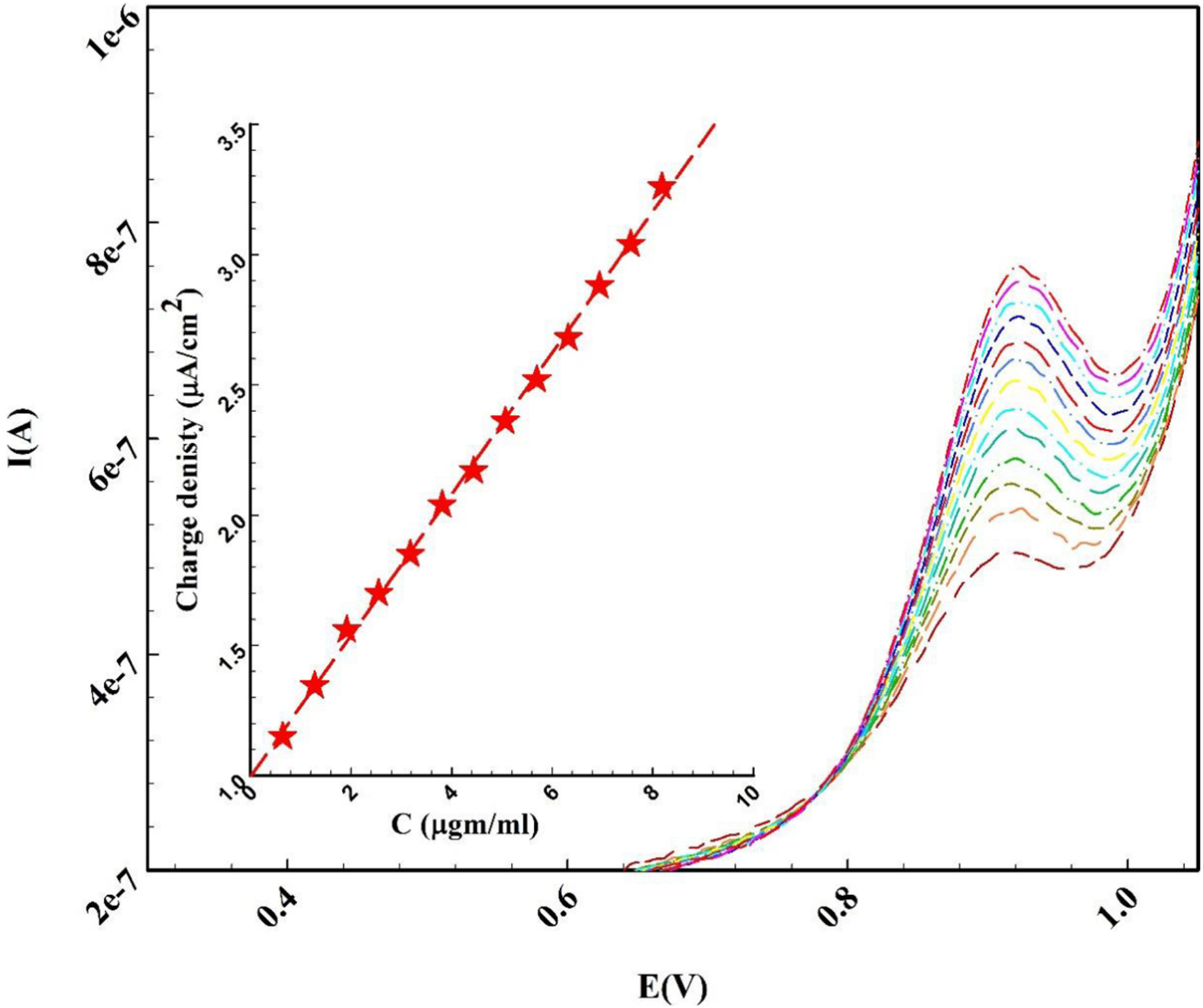
I(A)
1e-6
8e-7
6e-7
4e-7
2e-7
0.4
0.6
0.8
1.0
E(V)
Charge denisty (μA/cm2)
3.5
3.0
2.5
2.0
1.5
1.0
2
4
6
8
10
C (μgm/ml)

Figure 7

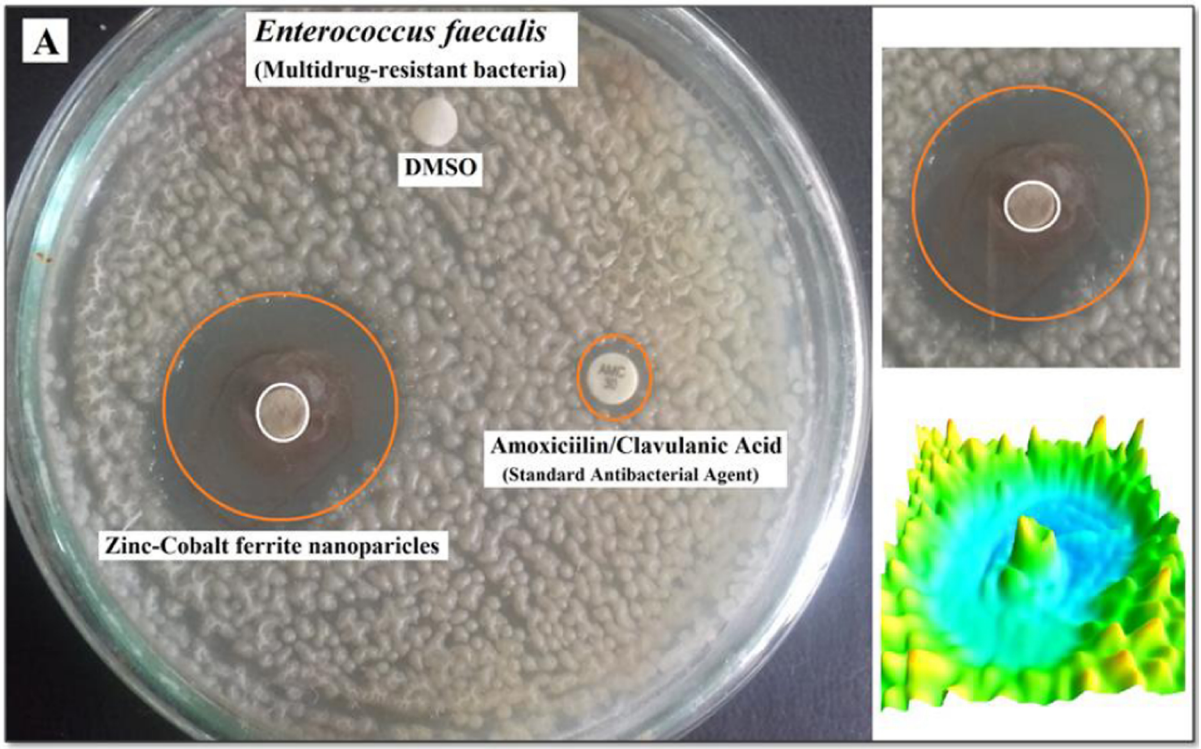
A
Enterococcus faecalis
(Multidrug-resistant bacteria)
DMSO
Amoxiciilin/Clavulanic Acid
(Standard Antibacterial Agent)
Zinc-Cobalt ferrite nanoparicles

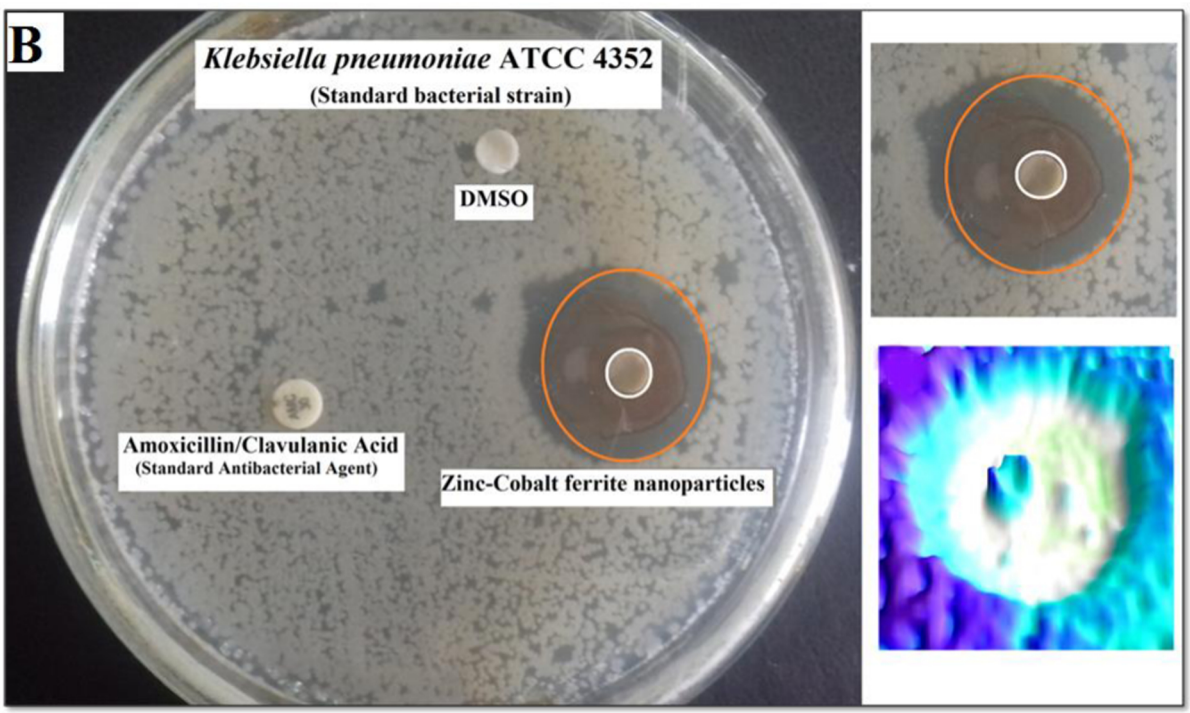
B
Klebsiella pneumoniae ATCC 4352
(Standard bacterial strain)
DMSO
Amoxicillin/Clavulanic Acid
(Standard Antibacterial Agent)
Zinc-Cobalt ferrite nanoparticles

Figure 8